

Geophysical Research Letters[®]



RESEARCH LETTER

10.1029/2025GL115919

Key Points:

- Heat flow is low in the Anhydros Basin, Aegean Sea
- Ocean bottom temperatures were cold during the last glacial
- Subsurface temperature records surface temperature changes and heat flow

Supporting Information:

Supporting Information may be found in the online version of this article.

Correspondence to:

M. Manga,
mmanga@berkeley.edu

Citation:

Manga, M., Tominaga, M., Preine, J., Ronge, T. A., Beethe, S., Hübscher, C., et al. (2025). Low heat flow in the Anhydros Basin, Aegean Sea, recorded by deep subsurface temperatures. *Geophysical Research Letters*, 52, e2025GL115919. <https://doi.org/10.1029/2025GL115919>

Received 13 MAR 2025

Accepted 21 MAY 2025

Author Contributions:

Conceptualization: Michael Manga

Data curation: Michael Manga





















Formal analysis: Michael Manga, Masako Tominaga, Jonas Preine, Thomas A. Ronge

Funding acquisition: Michael Manga
Investigation: Michael Manga, Sarah Beethe, Christian Hübscher, Iona McIntosh, Paraskevi Nomikou, Steffen Kutterolf, Tim Druitt, Alexis Bernard, Carole Berthod, Hehe Chen, Acacia Clark, Susan DeBari, Tatiana I. Fernandez-Perez, Ralf Gertisser, Raymond M. Johnston, Christopher K. Jones, K. Batuk Joshi, Günther Kletetschka, Olga Koukousioura, Molly McCanta, Antony Morris, Katharina Pank, Ally Peccia, Paraskevi N. Polymenakou, Adam Woodhouse, Yuzuru Yamamoto
Methodology: Michael Manga

© 2025. The Author(s).

This is an open access article under the terms of the [Creative Commons Attribution License](#), which permits use, distribution and reproduction in any medium, provided the original work is properly cited.

Low Heat Flow in the Anhydros Basin, Aegean Sea, Recorded by Deep Subsurface Temperatures

Michael Manga¹ , Masako Tominaga² , Jonas Preine^{2,3} , Thomas A. Ronge⁴, Sarah Beethe⁵ , Christian Hübscher³ , Iona McIntosh⁶ , Paraskevi Nomikou⁷ , Steffen Kutterolf⁸ , Tim Druitt⁹ , Alexis Bernard¹⁰, Carole Berthod¹¹ , Hehe Chen¹² , Acacia Clark¹³ , Susan DeBari¹⁴ , Tatiana I. Fernandez-Perez¹⁵, Ralf Gertisser¹⁶ , Raymond M. Johnston¹⁷, Christopher K. Jones¹⁸ , K. Batuk Joshi¹⁹ , Günther Kletetschka²⁰ , Olga Koukousioura²¹ , Molly McCanta²² , Antony Morris²³ , Katharina Pank⁸ , Ally Peccia²⁴ , Paraskevi N. Polymenakou²⁵, Adam Woodhouse²⁶ , and Yuzuru Yamamoto²⁷

¹Department of Earth and Planetary Science, University of California, Berkeley, CA, USA, ²Department of Geology and Geophysics, Woods Hole Oceanographic Institution, Woods Hole, MA, USA, ³Institute of Geophysics, University of Hamburg, Hamburg, Germany, ⁴Texas A&M University, College Station, TX, USA, ⁵College of Earth, Ocean, and Atmospheric Sciences, Oregon State University, Corvallis, OR, USA, ⁶Japan Agency for Marine-Earth Science and Technology, Yokosuka, Japan, ⁷Department of Geology and Geoenvironment, National and Kapodistrian University of Athens, Athens, Greece, ⁸GEOMAR Helmholtz Centre for Ocean Research Kiel, Kiel, Germany, ⁹Laboratoire Magmas et Volcans, University Clermont-Auvergne, CNRS, IRD, OPGC, Clermont-Ferrand, France, ¹⁰Laboratoire des Fluides Complexes et leurs Réservoirs, Université de Pau et des Pays de l'Adour, Pau, France, ¹¹Institut De Physique Du Globe De Paris, Centre National de la Recherche Scientifique (CNRS), Paris, France, ¹²School of Ocean Sciences, China University of Geosciences, Beijing, China, ¹³School of Natural Sciences/CODES, University of Tasmania, Hobart, TAS, Australia, ¹⁴Geology Department, Western Washington University, Bellingham, WA, USA, ¹⁵Department of Geology, Kent State University, Kent, OH, USA, ¹⁶School of Geography, Geology and the Environment, Keele University, Staffordshire, UK, ¹⁷School of Geosciences, University of South Florida, Tampa, FL, USA, ¹⁸Department of Earth and Planetary Sciences, University of California, Riverside, CA, USA, ¹⁹Department of Geology, Central University of Himachal Pradesh, Dharamshala, India, ²⁰USA and Faculty of Science, Geophysical Institute, University of Alaska Fairbanks, Fairbanks, AK 99709, Charles University, Prague, Czechia, ²¹School of Geology, Aristotle University of Thessaloniki, Thessaloniki, Greece, ²²Department of Earth and Planetary Sciences, University of Tennessee, Knoxville, TN, USA, ²³School of Geography, Earth and Environmental Sciences, Plymouth University, Plymouth, UK, ²⁴Lamont-Doherty Earth Observatory, Columbia University, Palisades, NY, USA, ²⁵Institute of Marine Biology, Biotechnology and Aquaculture, Hellenic Centre for Marine Research, Heraklion, Greece, ²⁶School of Earth and Environmental Sciences, Cardiff University, Cardiff, UK, ²⁷Graduate School of Science, Kobe University, Kobe, Japan

Abstract Subseafloor in situ temperatures in a drilled hole in the Anhydros Basin, Aegean Sea, measured during International Ocean Discovery Program (IODP) Expedition 398, yielded a low heat flow (<0.023 W/m²) despite active magmatism and rifting in the region. The coldest and highest temperatures were 13.9°C at 52.5 m below seafloor (mbsf) and 15.5°C for the deepest measurement at 360.4 mbsf, respectively. Comparison of a heat transfer model with measurements suggests that sea bottom temperatures during the last glacial period were up to 10°C cooler than Holocene temperatures. The magnitude of Holocene warming co-varies with the geothermal heat flow: if the former goes up the latter goes up. Low heat flow may arise from lateral removal of heat through deeper formations by gravity driven advection of fluids. Tectonic separation of the northwestern Anhydros Basin from the Christiana-Santorini-Kolumbo volcanic field may lead to minimal magmatic influences on heat flow.

Plain Language Summary Temperatures in Earth's crust reveal the processes that create and transport heat. In the rifting Anhydros Basin in the Aegean Sea, north of the active South Aegean Volcanic Arc, International Ocean Discovery Program Expedition 398 measured cold subsurface temperatures in a borehole to depths exceeding 300 m below the seafloor. These temperatures record low heat flow and cold seafloor temperatures from the last glacial period. The low heat flow at shallow depths may be due to deeper fluid circulation that removes heat. Low heat flow further implies that there are no magma bodies within the crust in the northwestern part of the Anhydros Basin.

Project administration: Michael Manga, Thomas A. Ronge, Steffen Kutterolf, Tim Druitt

Resources: Michael Manga

Software: Michael Manga

Supervision: Michael Manga, Thomas A. Ronge, Steffen Kutterolf, Tim Druitt

Validation: Michael Manga

Visualization: Michael Manga

Writing – original draft: Michael Manga, Tim Druitt

Writing – review & editing:

Michael Manga, Masako Tominaga,

Jonas Preine, Thomas A. Ronge,

Sarah Beethe, Christian Hübscher,

Iona McIntosh, Paraskevi Nomikou,

Steffen Kutterolf, Tim Druitt,

Ralf Gertisser, Olga Koukousioura

1. Introduction

Heat flow measurements are a window into the thermal structure and history of the lithosphere. Subsurface temperature measurements used to measure heat flow, however, are impacted by changes in surface temperature. Through thermal diffusion, temperature perturbations extend deeper as the duration of surface temperature changes becomes longer. Glacial-interglacial temperature changes, for example, affect temperatures to depths of hundreds of meters. Indeed, temperature measurements on land have been used to constrain temperature changes over the last glacial cycle (e.g., Beltrami et al., 2014). However, those temperature records are also affected by the background geothermal heat flux. Subsurface temperature measurements are a record of boundary conditions—surface temperature and its history, and heat flow at depth—with additional possible influences from advection of heat by fluid transport in the crust, sedimentation, and erosion.

Here we interpret temperature measurements made to a depth of 360 m in the Anhydros Basin north of the Christiana-Santorini-Kolumbo Volcanic Field in the South Aegean Volcanic Arc (Figure 1a) to understand the thermal structure of the crust. Though deep below the sea floor compared to typical measurements with Lister-type heat flow probes, the temperature measurements still contain a record of both the change in ocean bottom temperature during the Holocene and the regional heat flow.

The Anhydros Basin spans from the northeast of Santorini toward the island of Amorgos and contains the submarine Kolumbo Volcano and the Kolumbo Volcanic Chain with more than 20 submarine volcanic edifices (Figure 1b). Bounded by the Ios Fault, the northeastern part of the Anhydros Basin is a tectonic half-graben (Figure 1c) that experienced episodic rifting (Hübscher et al., 2015; Preine, Karstens, et al., 2022). International Ocean Discovery Program (IODP) Expedition 398 to the Hellenic Arc sought to understand the volcanic history of this arc, the connection between magmatic and rifting processes, and the current and past submarine environments in an active volcanic arc (Druitt, Kutterolf, Ronge, & the Expedition 398 Scientists 2024). This volcanic field evolved since the Late Pliocene and produced numerous explosive eruptions during the Quaternary, depositing thick volcanic deposits in the adjacent rift basins (e.g., Druitt et al., 1999; Druitt, Kutterolf, Ronge, Hübscher, et al., 2024; Preine, Hübscher, et al., 2022; Karstens, Crutchley, et al., 2023; Karstens, Preine, et al., 2023). The volcanic centers formed and evolved in an active rift environment (e.g., Nomikou et al., 2019; Preine, Karstens, et al., 2022) and volcanism and tectonics have been proposed to influence each other (Crutchley et al., 2023; Heath et al., 2019; Preine, Karstens, et al., 2022).

2. Background and Methods

IODP Expedition 398 was conducted to obtain the seafloor record of feedbacks between volcanism, magmatism, crustal tectonics, sea level change, and the deep biosphere within the southern Aegean Sea and inside and outside Santorini caldera. Subsurface temperature measurements have a fundamental scientific significance for several objectives of IODP Expedition 398. Temperature gradients can provide insight into regional heat flow and hence the structure of the lithosphere and presence and cooling of subsurface magma bodies that in turn affect habitability and the geochemical and diagenetic processes in these marine sediments. Subsurface temperatures can also record past sea bottom temperatures and preserve a record of a changing climate.

Drilling and coring unconsolidated volcanoclastic materials turned out to be challenging as the holes are prone to collapse and the drill string can become stuck (e.g., Jutzeler et al., 2014; Jutzeler et al., 2025). Consequently, even though temperature measurements were initially planned at all sites, measurements were only made at the first site (U1589) and attempted only once at the second site (U1590).

Site U1589 is located at a water depth of 494 m below sea level (mbsl), about 10 km southwest of Amorgos Island in the northeastern Anhydros Basin (36°43.8'N, 25°38.9'E; Figure 1). The Site targets the volcanoclastic sediment delivered from Santorini and Kolumbo volcanoes by submarine flows and subaerial tephra falls. The setting also enables the study of the relationships between rifting and volcanism. Three holes, A, B and C, were drilled to a maximum recovery depth of 621.9 mbsf (Druitt, Kutterolf, Ronge, & the Expedition 398 Scientists 2024). Measurement methods and uncertainties are presented in Kutterolf et al. (2024).

2.1. Temperature Measurements in Boreholes

Advanced Piston Coring was used in Holes U1589A and U1589B. Measurements were made with the Third-Generation, Advanced Piston Corer Temperature Tool (APCT-3) that records temperature with a thermistor at

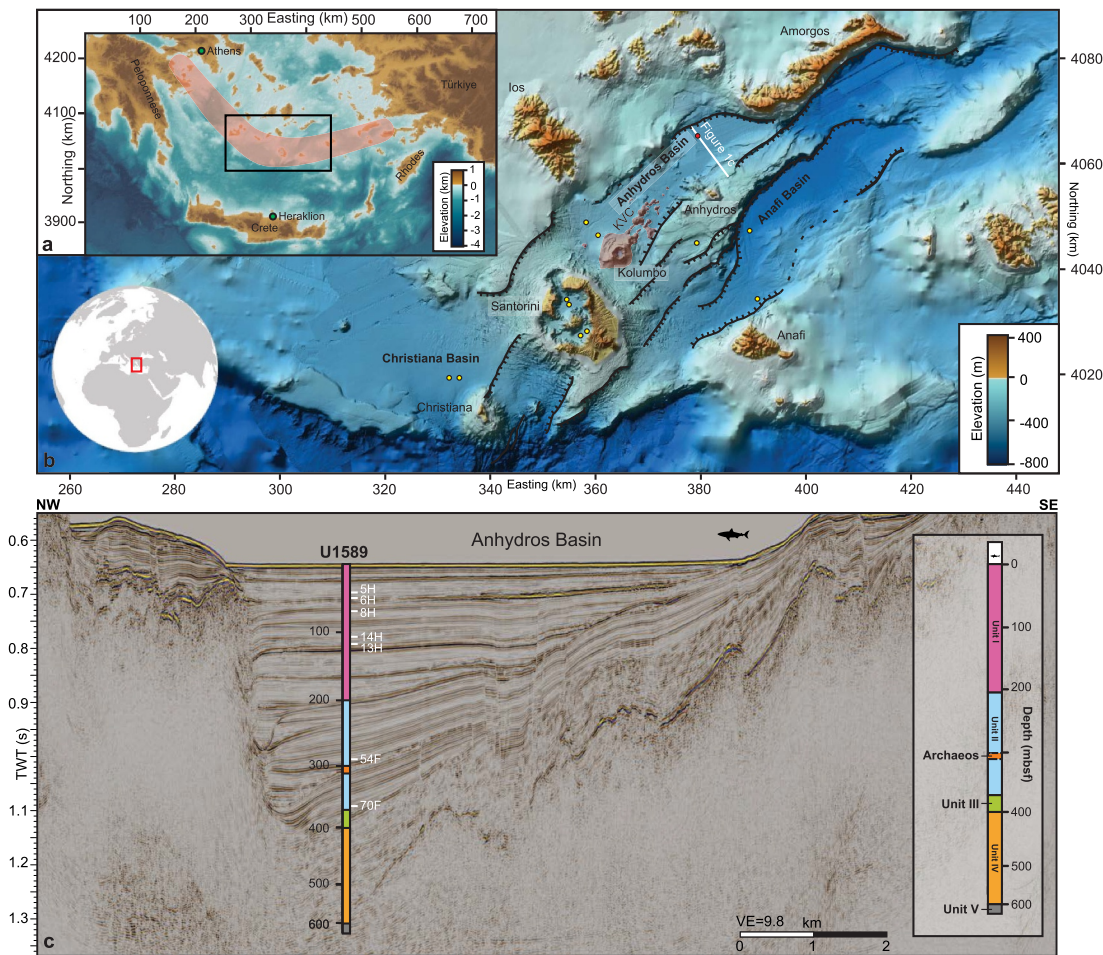


Figure 1. (a) Regional map of the southern Aegean Sea highlighting the South Aegean Volcanic Arc (shaded in red). The black box indicates the study area, and major coastal cities in the Aegean are marked with green circles. The coordinate system used here and in all following maps is UTM Zone 35N, WGS84 datum. (b) Morphological map of the Christiana-Santorini-Kolumbo Rift Zone. Circles show International Ocean Discovery Program Expedition 398 drill sites. The red circle indicates Site U1589. White line indicates location of seismic profile GEOMAR_5016 shown in (c). Bathymetry from Nomikou et al. (2012, 2013, 2018) and Hooft et al. (2017). (c) Seismic cross-section of the northeastern Anhydros Basin crossing Site U1589 (Karstens et al., 2020). Colors indicate lithologies of Site U1589. Unit I: Volcanic sediments; Unit II: Ooze and calcareous mud; Unit III: Siliciclastics with shells; Unit IV: Oxidized conglomerate, breccia and sandstone; Unit V: Carbonate rocks. Archaeos Tuff depth is from Druitt, Kutterolf, Ronge, Hübscher, et al. (2024). Horizons after Preine, Hübscher, et al. (2022); Preine, Karstens, et al. (2022) and core-seismic integration from Preine et al. (2025). TWT: Two way travel time. White labels indicate cores and depths of temperature measurements. Vertical exaggeration is 9.8.

the outside edge of the cutting shoe (Heesemann et al., 2008). After the APCT-3 tool penetrates the sediment, it is held in place for about 10 min while it records temperature at 1 Hz. The Sediment Temperature 2 (SET2) tool was used in Hole U1589B (iodp.tamu.edu/tools/logging/index.html). The SET2 tool records in situ temperature with a thermistor located 1 cm from the probe tip. The probe tip contains both the data logger and the thermistor string and is designed to enter the sediment with minimal disturbance.

The recorded decay of temperature from each of these measurements is fit to a theoretical solution of the temperature equilibration using the code TP-Fit (Fisher et al., 2007). The calculated temperature depends on the thermal conductivity, density, and specific heat capacity of the surroundings. In modeling the temperature decay, we use a thermal conductivity $k = 1.0 \text{ W m}^{-1} \text{ K}^{-1}$ and a product of density and specific heat of $\rho C = 3.7 \times 10^6 \text{ J m}^{-3} \text{ K}^{-1}$ for APCT-3 measurements, and $k = 1.2 \text{ W m}^{-1} \text{ K}^{-1}$ and $\rho C = 3.7 \times 10^6 \text{ J m}^{-3} \text{ K}^{-1}$ for SET2 measurements at greater depths. An uncertainty in k of $\pm 0.15 \text{ W m}^{-1} \text{ K}^{-1}$ and in ρC of $\pm 0.3 \times 10^6 \text{ J m}^{-3} \text{ K}^{-1}$ are adopted to calculate the uncertainty in temperature. We use combinations of upper and lower bounds on k and ρC to find the highest and lowest temperature fits to the data and use one half of the maximum difference as our

estimate of the uncertainty in the calculated temperature. The uncertainty on in situ temperature measurements with this approach is usually $<0.2^{\circ}\text{C}$.

2.2. Thermal Conductivity and Heat Production Data on Cored Materials

Thermal conductivity was measured on seawater-saturated split cores from the working halves (sample size ≥ 6 cm) using the TeKa TK04 system (Blum, 1997). All measurements were made after the core equilibrated with the ambient temperature in the ship's laboratory. Reported values are the average of three repeat measurements separated in time by 10 minutes. Accuracy was assessed by measuring a standard.

The concentration of heat producing elements U, Th and K were extracted from Natural Gamma Radiation (NGR) spectra measured at 10 cm intervals on whole cores, using the modeling approaches and workflow in Vleeschouwer et al. (2017). The mean concentrations averaged between 0 and 514.5 mbsf are 0.733 weight %, 4.19 ppm and 1.24 ppm for K, Th and U, respectively.

2.3. Heat Flow Modeling

To interpret the temperature measurements in terms of both changes in ocean temperature and the geothermal heat flow, we model heat transfer in a compacting sediment column. We neglect any fluid flow except for that driven by compaction. We assume all motion and heat transfer occur in the vertical (z) direction. The proximity of the shallow limestone basement west of the fault leads to heat refraction but only small perturbations to vertical heat conduction at Site U1589 (Figures S1 and S2 in Supporting Information S1).

Heat transfer is governed by the advection-diffusion equation

$$\overline{\rho C} \frac{\partial T}{\partial t} = \frac{\partial}{\partial z} \left[\bar{k} \frac{\partial T}{\partial z} \right] - \overline{\rho C u} \frac{\partial T}{\partial z} + \bar{A} \quad (1)$$

where the overbar indicates bulk quantities, T is temperature, t is time, k is thermal conductivity, ρ is density, C is heat capacity, u is velocity (defined later in terms of sediment and fluid velocity), and A is the volumetric heat production rate. k is based on measurements from recovered cores.

The bulk quantities in Equation 1 depend on porosity ϕ and are given by

$$\overline{\rho C} = \rho_w C_w \phi + \rho_s C_s (1 - \phi) \quad (2)$$

$$\overline{\rho C u} = \rho_w C_w \phi u_w + \rho_s C_s (1 - \phi) u_s \quad (3)$$

where subscripts w and s denote water and sediment values, respectively. We use $C_s = 1 \text{ kJ kg}^{-1} \text{ K}^{-1}$, and standard values for seawater.

We calculate the heat production A in units of W m^{-3} from the NGR measured concentrations of K, U and Th (Section 2.2) using

$$A = 10^{-11} [\rho_w \phi + \rho_s (1 - \phi) (9.52 c_U + 2.56 c_{Th} + 3.48 c_K)] \quad (4)$$

where c_U and c_{Th} are the concentrations of U and Th in ppm, respectively, and c_K is the concentration of K in weight percent (Rybach, 1988).

Porosity decreases exponentially with depth

$$\phi(z) = \phi_0 e^{-\lambda z} \quad (5)$$

with parameters in (5) obtained from our measurements on recovered cores.

Conservation of mass for water and sediment allows us to compute u_s and u_w

$$\frac{d}{dz}[\rho_s u_s (1 - \phi)] = 0 \quad (6)$$

and

$$\frac{d}{dz}[\rho_w u_w \phi] = 0 \quad (7)$$

Equations 6 and 7 can be solved with the boundary condition that the sedimentation rate at the seafloor is u_{s0} and that at $z = B$, $u_w(z = B) = u_s(z = B)$, to give

$$u_s(z) = u_{s0} \frac{1 - \phi_0}{1 - \phi(z)} \quad (8)$$

and

$$u_s(z) = u_{s0} \frac{1 - \phi_0}{1 - \phi_B} e^{\lambda(z-B)} \quad (9)$$

We solve Equation 1 explicitly with a second order finite-difference method (Manga, 2025), use a 1 m spatial resolution, and obtain parameters in Equations 1–3 and 5 from measurements reported in Section 3.1.

3. Results

3.1. Thermal Conductivity and Porosity

A total of 91 thermal conductivity measurements were made on cored samples from Site U1589 (Druitt, Kutterolf, Ronge, & the Expedition 398 Scientists 2024). Overall, thermal conductivity k increases with depth (Figure 2a). A least-squares linear fit to all the thermal conductivity data is

$$k(z) = (0.804 \pm 0.032) + (0.00167 \pm 0.00013)z \quad (10)$$

with z in m and k in $\text{Wm}^{-1}\text{K}^{-1}$. Thermal conductivity could not be measured on very coarse, permeable samples of pumice lapilli. Thus, an inherent sampling bias may affect mean values, variability, and trends. In the thermal models we use Equation 10 for k up to $2.0 \text{ Wm}^{-1}\text{K}^{-1}$ and a value of $2.0 \text{ Wm}^{-1}\text{K}^{-1}$ for greater depths.

Discrete porosity measurements were made on 192 samples. Porosity decreases with depth (Figure 2b). In the heat flow simulations, we use $\phi_0 = 0.7$, $\lambda^{-1} = 1.3 \text{ km}$ (shown with the black curve in Figure 2b) and $B = 380 \text{ m}$.

3.2. Downhole Temperature Measurement

Temperature was measured by the APCT-3 tool at the bottom of Cores 4, 7, 10 and 13 in Hole U1589A, at 30.7, 59.2, 87.7 and 116.3 mbsf, respectively, and the bottom of Cores 5, 6, 8, 11 and 14 in Hole U1589B at 43.0, 52.5, 71.5, 85.7, and 105.6 mbsf, respectively (Druitt, Kutterolf, Ronge, Beethe, et al., 2024). The SET2 tool was deployed at the bottom of Cores 54 and 70 in Hole U1589B, at 288.2 and 360.4 mbsf, respectively (Druitt, Kutterolf, Ronge, Beethe, et al., 2024). The temperature of ocean water at the seafloor was $15.47 \pm 0.05^\circ\text{C}$ based on mudline temperature measurements from Core U1589B-14H (Table S1 in Supporting Information S1; Druitt, Kutterolf, Ronge, Beethe, et al., 2024). Figure 3 and Table S1 in Supporting Information S1 summarize the measurements.

Measurements can be compromised by tool movement because of ship heave and low friction in the upper part of the borehole, as seen in the data from the APCT-3 in Figure S3 in Supporting Information S1 where the monotonic decay of temperature is disrupted. Because of the very long extrapolation in time needed to obtain the formation temperature from the short time window during which the probes are deployed, we do not calculate formation temperatures or interpret their values when temperature measurements show clear disruptions in the time series (all data are shown in Figure S4 in Supporting Information S1). Cracked formations in the stiffer sediments in which the SET2 tool was used could also lead to anomalously low temperatures by permitting downward

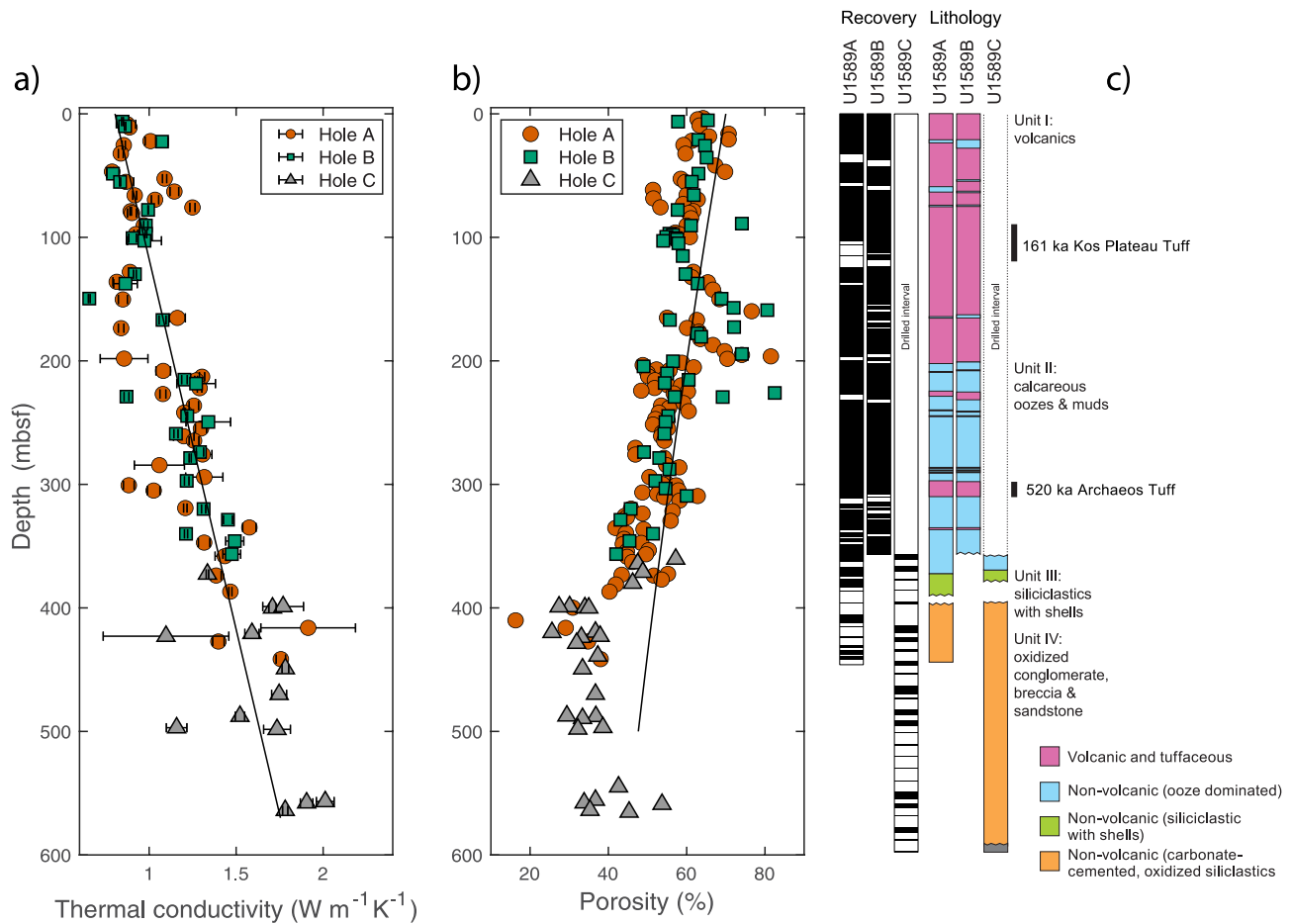


Figure 2. (a) Thermal conductivity measurements on working half sections from Site U1589. Black solid line shows the least-squares best linear fit to all the data. Symbols: red = Hole A, green = Hole B, and gray = Hole C. (b) Porosity measured on discrete samples along with the exponential model used in the heat flow simulations. (c) Units and lithologies based on core descriptions, with recovered records in black and gaps in white, and the ages and depths of two large volcanic tuffs indicated with names and ages. Gray at the bottom is basement.

circulation of cold water. Based on the cores that were recovered and the smoothly evolving temperatures recorded by the SET2 tool, there is no clear reason to discount the data, but we remain cognizant of possible measurement biases (e.g., Neumann et al., 2023).

3.3. Heat Flow Models

For the time-averaged sediment accumulation rate, we use the 300 mbsf depth of the Archaeos Tuff and its biostratigraphically estimated age of 520 ka (Druitt, Kutterolf, Ronge, Hübscher, et al., 2024). Despite the very high sedimentation rate, owing to the time period of sediment accumulation and compaction, sediment burial and compaction have small effects on the computed temperature distributions (Hutchison, 1985; Manga et al., 2012; see Figure S6 in Supporting Information S1 for other ages) but are still accounted for in the model.

In the absence of measured or proxy seafloor temperature variations on seasonal, historic, and prehistoric timescales near Site U1589, we need to adopt temperature values and histories as boundary conditions. We begin the simulations at 300 ka with a steady temperature for a specified basal heat flux q_0 and surface temperature $T_s = 14^\circ\text{C} - \Delta T$. We then solve Equation 1 accounting for sedimentation and compaction. At 12 ka, we increase the temperature by an amount ΔT . Over the most recent 100 years, we increase the surface temperature from 14°C to 15.5°C to approximate the effects of anthropogenic warming (Figure S5 in Supporting Information S1). The RV Poseidon POS510 cruise used a GDY heat probe to measure temperature in the upper less than 3 m of sediment in the Cyclades back-arc basin (Hannington et al., 2018); in the Anhydros Basin at 3 locations with water depths of 446–473 mbsl, temperature was 15.38 – 15.23°C , similar to our measurement and our adopted

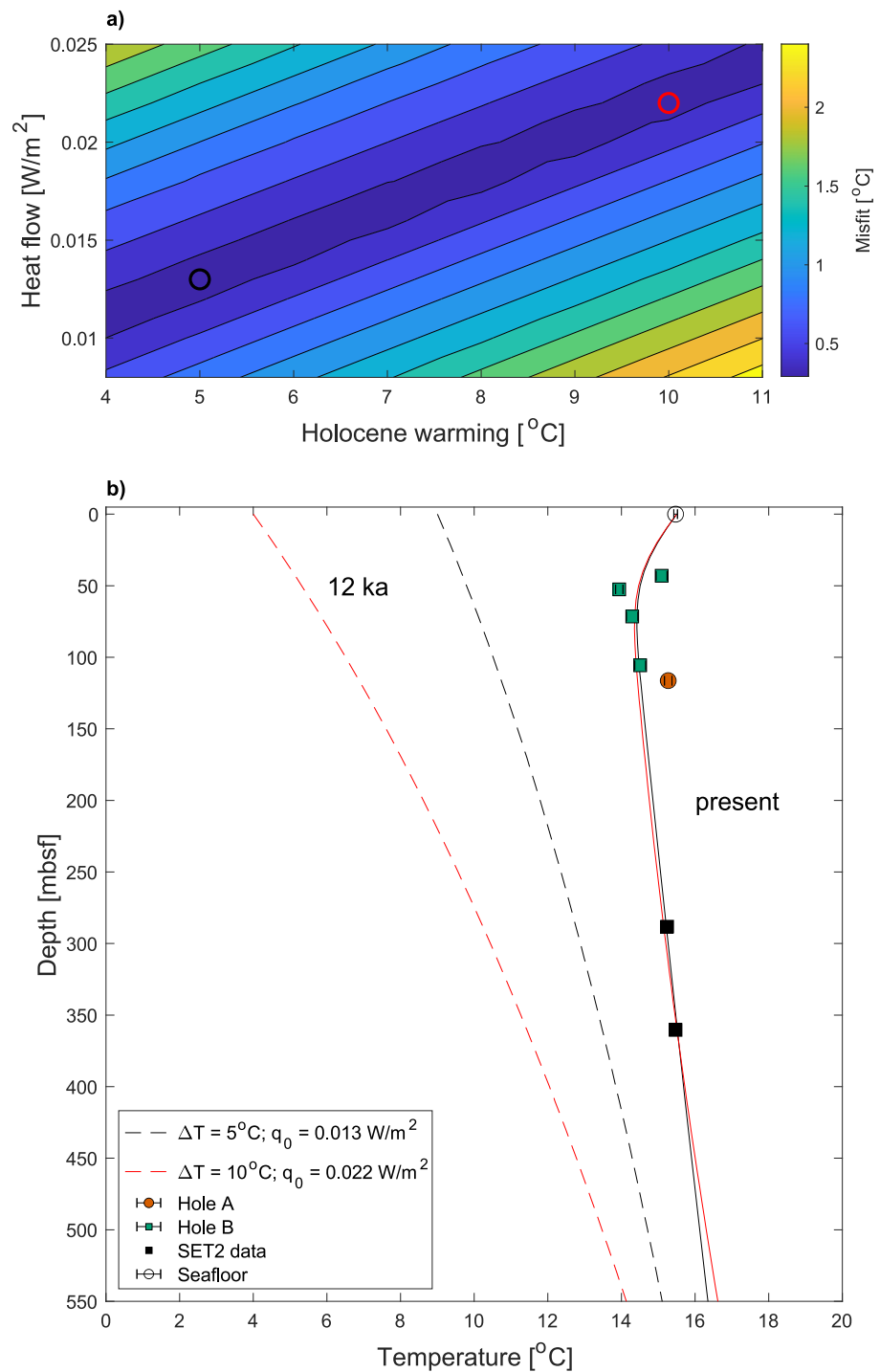


Figure 3. (a) Mean absolute value of the temperature difference between the computed present-day hole temperatures and the model as a function of the magnitude of Holocene warming and background heat flow. The red and black circles indicate the parameter values used for the example geotherms in panel (b). (b) Temperature as a function of depth at Site U1589. Legend identifies the hole and measurements made with the Sediment Temperature 2 (SET2) tool. The red and black curves show the pre-Holocene and present-day temperatures for the parameter values listed in the legend. Plotted data are tabulated in Table S1 in Supporting Information S1.

present-day boundary condition. Anthropogenic warming influences depths shallower than where we have subsurface temperature measurements but connects our deeper measurements to the measured seafloor temperature. Both the 14°C and recent 1.5°C of warming were chosen to match the lowest measured temperature and shallow temperatures that serve as boundary conditions to interpret deeper measurements.

Figure 3 shows the relationship between the temperature change and heat flow and the fit to the temperature measurements. Misfit is quantified as the average absolute value of the difference between the measurements and simulation. There is a relationship between the background heat flow and the magnitude of Holocene warming: as ΔT increases, the measurements accommodate larger heat flows q_0 . Two examples of good fits for $\Delta T = 5^\circ\text{C}$ and $q_0 = 0.013 \text{ W/m}^2$, and $\Delta T = 10^\circ\text{C}$ and $q_0 = 0.023 \text{ W/m}^2$ are shown in Figure 3b. If we neglect the SET2 measurements when comparing the simulations and data, we obtain similar results for ΔT and q_0 (Figure S6 in Supporting Information S1).

4. Discussion

For the possible range of ΔT , the temperature measurements suggest low geothermal heat flows q_0 (Figure 3a) well below the mean continental value of 0.065 W/m^2 (Davies, 2013). We thus discuss the origins of the cool temperatures and low implied heat flow.

4.1. Magnitude of Holocene Warming

Subsurface temperatures are impacted by surface temperature and its changes over time. In deep ocean settings that can be accessed by deep water formed at polar latitudes, the ocean bottom temperature remains close to isothermal. In shallower marine settings such as those cored by Expedition 398 in the Eastern Mediterranean, temperature fluctuations can be greater than a few degrees between glacial and interglacial periods (e.g., Kuhnt et al., 2008; Pasquale et al., 2005) and these affect the subsurface temperatures we measured. The depths impacted by changing temperatures depend on the time scale for the temperature variations. Consider a sea bottom temperature that varies periodically with frequency ω (and period $\tau = 2\pi/\omega$) such that $T(z=0, t) = T_0 + \Delta T \cos(\omega t)$, where z is depth below the seafloor, T_0 is the mean temperature of the seafloor, and ΔT is the magnitude of the temperature variations. For assumed constant thermal diffusivity κ , the solution to the one-dimensional diffusion equation (Equation 1 neglecting compaction and heat production, and for constant material properties) is

$$T(z, t) = T_0 + \Delta T e^{-z\sqrt{\omega/2\kappa}} \cos\left(\omega t - z\sqrt{\omega/2\kappa}\right). \quad (11)$$

The depth D to which temperature variations are reduced in amplitude by a factor of e is thus $D = \sqrt{2\kappa/\omega}$. Annual temperature variations have $D = 1.7 \text{ m}$ for $\kappa = 2.7 \times 10^{-7} \text{ m}^2 \text{ s}^{-1}$, and thus will not affect temperatures at our measurement depths. However, changes from anthropogenic warming that reach the seafloor will affect the upper few tens of meters (Figure 3). The larger amplitude changes from Quaternary glacial cycles ($\tau = 10^5$ years) have $D = 0.52 \text{ km}$. This depth is greater than the depth extent of our measurements, and the cool temperatures we measured thus contain record of cold temperatures from the last glacial period superimposed on the geothermal gradient (with neither ΔT nor the geothermal gradient directly measured).

Paleotemperatures from various proxies show large variations in the inferred temperature during the last glacial throughout Europe. For example, Last Glacial Maximum (LGM) cooling of $\sim 9^\circ\text{C}$ in the Paris Basin, Western Europe, was inferred from noble gas paleothermometry (Bekaert et al., 2023). Paleotemperature reconstructions with data assimilation have smaller cooling near the Mediterranean than in northern and continental Europe (Tierney et al., 2020). Sea-surface eastern Mediterranean temperatures (SST) during the LGM based on planktonic foraminifera were 5°C (summer) to 7°C (winter) cooler (Hayes et al., 2005). Aksu et al. (1995) estimate $5\text{--}10^\circ\text{C}$ of SST warming from 14 ka to 9.6 ka from a collection of proxy data in the Aegean.

Our measurements, if reliable, are a direct measure of local changes in temperature. But there is a correlation with heat flow leading to a non-unique interpretation of the geothermal gradient. Future paleoproxy bottom water temperatures measurements from U1589 cores would constrain ΔT and thus the heat flow (Figure 3a).

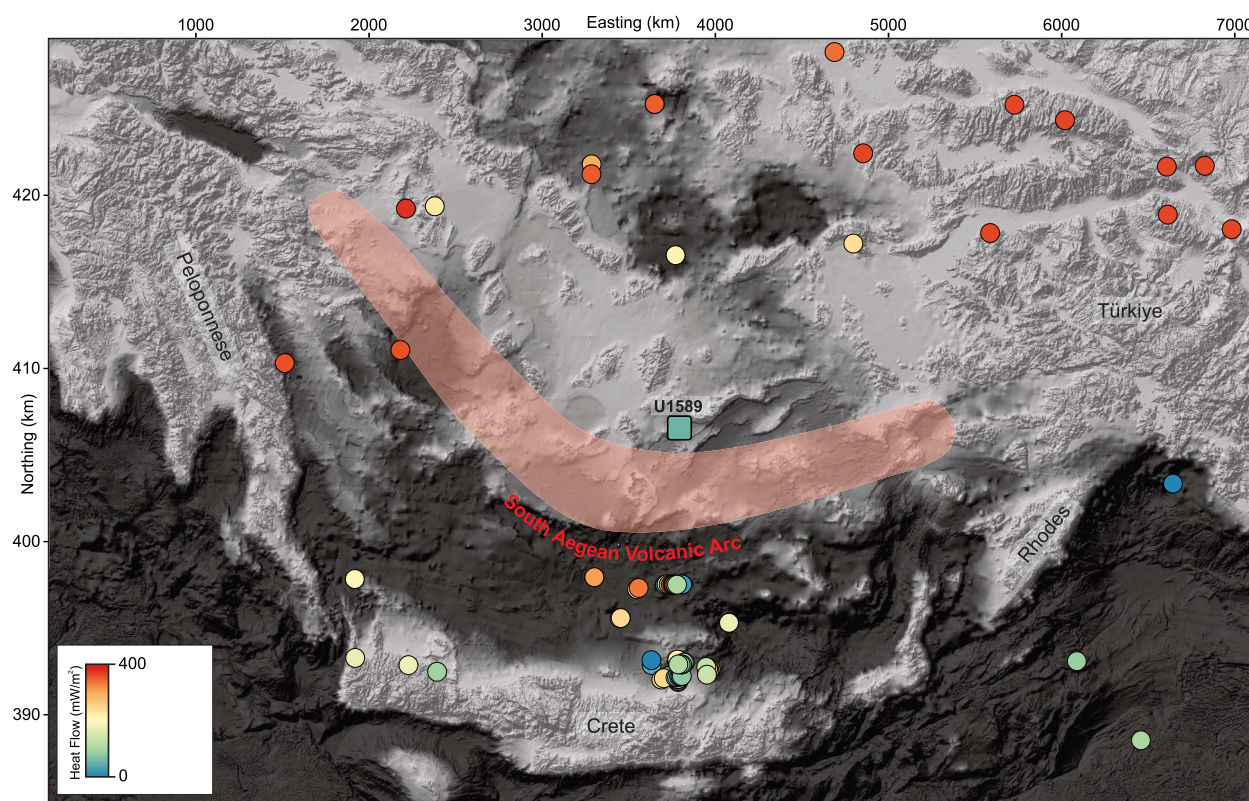


Figure 4. Regional map of the southern Aegean Sea with available heat flow measurements shown with circles, colored by the value of heat flow (Global Heat Flow Data Assessment Group et al., 2024). The square indicates the heat flow measured at Site U1589. The location of the South Aegean Volcanic Arc is shaded in red. Bathymetry is a greyscale version of that shown in Figure 1a.

4.2. Interpretations of Low Heat Flow

Conductive regional heat flows can exceed 0.1 W/m^2 in volcanic arcs, including submarine volcanic arcs such as the Lesser Antilles (e.g., Manga et al., 2012). Regions of extending continental crust such as the Basin and Range, USA also have similarly high heat flows that can exceed 0.1 W/m^2 (e.g., Blackwell, 1983). Our inferred heat flows of $<0.023 \text{ W/m}^2$ are thus low compared to similar tectonic settings and the continental average (Davies, 2013; Pollack et al., 1993).

Our low temperatures differ from those from the nearest other deep temperature measurements. Deep Sea Drilling Project (DSDP) Leg 42A Site 378 was drilled in the Cretan Basin, 60 km south-southwest of Santorini, at 1835 mbsl. A temperature of 35°C was reached at a depth of 302.5 mbsf, implying temperature gradients close to 60°C/km (Erickson and Herzen, 1978). Site 374 (DSDP Leg42A) in the Ionian Sea has a geothermal gradient of 28°C/km . Site 376 (DSDP Leg42A) on the Florence Rise between the Antalya and Levantine Basins, west of Cyprus, shows cool temperatures of 15°C at a depth of 131 mbsf (Erickson and Herzen, 1978). Figure 4 shows our inferred heat flow along with other regional estimates.

One possible explanation for the low inferred heat flow is that deeper formations (Units III and IV in Figures 1c and 2c), and perhaps the Archaeos Tuff, serve as pathways for gravity driven fluid circulation. Fluid advection can alter subsurface temperatures by transporting heat and has been documented in other submarine volcanic arc settings (e.g., Hornbach et al., 2024) and convergent margins where low heat flow has been attributed to vigorous fluid circulation (Davis et al., 1999; Harris et al., 2010). In the Anhydros Basin, cool surface waters could recharge in the southeast of the basin and discharge along the normal fault in the northwest. Future advective and diffusive fluid flow modeling of pore water geochemical profiles from Site U1589 cores could test for lateral advection by examining chloride, lithium, and strontium concentration gradients, which should show systematic deviations from diffusion profiles if significant lateral flow is present. Solid phase investigations of mineral alteration and/or authigenic mineral formation could constrain additional sources and sinks of relevant pore water constituents.

Regional scale advection through permeable formations leads to low surface heat flow, and occurs in many basins (e.g., Förster & Merriam, 1999; Manga, 1998) and seems a plausible explanation for the low inferred heat flow. On the other hand, published seismic imaging provides no evidence for undercompaction, drainage structures, or fluid flow, including no indication of ascent zones (pipes), polygonal faults, or lateral amplitude differences that arise from fluid flow (Hübscher et al., 2015; Preine, Hübscher, et al., 2022). We thus consider other possible contributions to the low heat flow.

The near surface geothermal heat flow contains a combination of heat produced by radiogenic elements, heat conducted through the lithosphere, and heat transferred from any magmatic bodies in the crust. Three non-advective factors can contribute to lowering heat flow. First, the site is in a portion of the Anhydros Basin far enough from the active arc and seafloor volcanism represented by a series of submarine cones of Kolumbo volcanic chain. The location of site U1589 in the Anhydros Basin is about 15 km from the northernmost Kolumbo submarine cone (Nomikou et al., 2013, 2016). The low measured heat flow may indicate that the deeper magmatic system creating the chain of Kolumbo cones does not extend as far northeast as site U1589 and that the lithosphere in this part of the Anhydros Basin is distinct from that hosting the Kolumbo volcanic chain (Figure 1b). Indeed, upper crustal magma reservoirs do not extend this far (McVey et al., 2020). Seismic imaging, including p-wave tomography and reflection seismic data, suggest a separation of the eastern and western Anhydros Basin, with a prominent basement rise separating both subbasins and limiting the extent of volcanism to the northeast (Heath et al., 2019; Nomikou et al., 2018; Preine, Karstens, et al., 2022). Second, the crust is thinner than average continental crust, 18 km at the drilled site compared to 40 km within the adjacent Greece (e.g., Makris et al., 2013), but the extension is young. East-west extension dates to the late Pliocene (e.g., Armijo et al., 1992), and much of the displacement on the Anhydros Basin bounding normal fault is Quaternary (Nomikou et al., 2018; Preine, Karstens, et al., 2022). Third, ophiolitic rocks and metamorphosed mafic rocks that make up much of the regional crust can be significantly less radiogenic than average crust (e.g., Hasterok et al., 2018; Pasquale et al., 2001). Assuming $q_0 = 0.023 \text{ W/m}^2$ ($\sim 10^\circ\text{C}$ Holocene warming) and a mantle heat flow of 0.011 W/m^2 (Hacker et al., 2011), and a crust thickness of 18 km, the volumetric heat production of $0.7 \mu\text{Wm}^{-3}$ is similar to some crustal averages (Taylor & McLennan, 1995) though probably lower than the global crustal mean (Rudnick & Fountain, 1995).

5. Conclusions

In the Anhydros Basin, ~ 20 km northeast of the Kolumbo volcanic field, close to isothermal conditions were measured as deep as 360 m below the seafloor, with a gradient of $\sim 3^\circ\text{C/km}$ at those depths. Temperature measurements record cool subsurface conditions for microbial communities and diagenetic processes, possibly explaining the lack of lithification observed in cored sediments. If heat conduction and sediment compaction are the only processes driving heat transfer, and the measurements are reliable, the low temperatures can be explained by both cool seafloor temperatures during the last glacial period, up to 10°C cooler than at present, combined with a low geothermal heat flux of $<0.23 \text{ W/m}^2$. The low geothermal heat flow may arise from basin-scale subsurface fluid advection. It also suggests this part of the basin is tectonically separated from the volcanic field. Low heat flow further implies that there are no magma bodies within the crust in the northwestern part of the Anhydros Basin.

Data Availability Statement

All data shown in figures are available through Druitt, Kutterolf, Ronge, Beethe, et al., 2024. The fortran77 code for computing misfit (Figure 3) and 2D temperature distribution (Figure S1 in Supporting Information S1) are provided in Manga (2025).

References

- Aksu, A. E., Yaşar, D. O. Ğ. A. N., Mudie, P. J., & Gillespie, H. (1995). Late Glacial-Holocene paleoclimatic and paleoceanographic evolution of the Aegean Sea: Micropaleontological and stable isotopic evidence. *Marine Micropaleontology*, 25(1), 1–28. [https://doi.org/10.1016/0377-8398\(94\)00026-J](https://doi.org/10.1016/0377-8398(94)00026-J)
- Armijo, R., Lyon-Caen, H., & Papanastassiou, D. (1992). East-West extension and Holocene normal-fault scarps in the Hellenic arc. *Geology*, 20(6), 491–494. [https://doi.org/10.1130/0091-7613\(1992\)020<0491:EWEAHN>2.3](https://doi.org/10.1130/0091-7613(1992)020<0491:EWEAHN>2.3)
- Bekaert, D. V., Blard, P. H., Raoult, Y., Pik, R., Kipfer, R., Seltzer, A. M., et al. (2023). Last glacial maximum cooling of 9°C in continental Europe from a 40 kyr-long noble gas paleothermometry record. *Quaternary Science Reviews*, 310, 108123. <https://doi.org/10.1016/j.quascirev.2023.108123>

Acknowledgments

We thank the crew, staff, and technicians of JOIDES Resolution Expedition 398, in particular Jurie Kotze, Etienne Claasen, and Zenon Mateo. We acknowledge travel support for US scientists by USSSP, as well as European scientists by IODP-Germany and ECORD, and the Université Clermont Auvergne in France. M. Manga received additional support from the Miller Institute and CIFAR Earth4D. G. Kletetschka was supported by the Czech Science Foundation (Grant 23-06075S). We thank T. Williams, G. Beardsmore, and an anonymous reviewer for constructive and insightful suggestions.

- Beltrami, H., Matharoo, G. S., Tarasov, L., Rath, V., & Smerdon, J. E. (2014). Numerical studies on the impact of the last glacial cycle on recent borehole temperature profiles: Implications for terrestrial energy balance. *Climate of the Past*, 10(5), 1693–1706. <https://doi.org/10.5194/cp-10-1693-2014>
- Blackwell, D. D. (1983). Heat flow in the northern basin and range province. *Geothermal Resources Council Special Report*, 13, 81–92.
- Blum, P. (1997). *Physical properties handbook: A guide to the shipboard measurement of physical properties of deep-sea cores*. Ocean Drill. Program.
- Crutchley, G. J., Karstens, J., Preine, J., Hübscher, C., Fossen, H., & Kühn, M. (2023). Extensional faulting around Kolumbo volcano, Aegean Sea—Relationships between local stress fields, fault relay ramps, and volcanism. *Tectonics*, 42(10), e2023TC007951. <https://doi.org/10.1029/2023TC007951>
- Davies, J. H. (2013). Global map of solid Earth surface heat flow. *Geochemistry, Geophysics, Geosystems*, 14(10), 4608–4622. <https://doi.org/10.1002/ggge.20271>
- Davis, E. E., Chapman, D. S., Wang, K., Villinger, H., Fisher, A. T., Robinson, S. W., et al. (1999). Regional heat flow variations across the sedimented Juan de Fuca Ridge eastern flank: Constraints on lithospheric cooling and lateral hydrothermal heat transport. *Journal of Geophysical Research*, 104(B8), 17675–17688. <https://doi.org/10.1029/1999JB900124>
- De Vleeschouwer, D., Dunlea, A. G., Auer, G., Anderson, C. H., Brumsack, H., de Loach, A., et al. (2017). Quantifying K, U, and Th contents of marine sediments using shipboard natural gamma radiation spectra measured on DV JOIDES Resolution. *Geochemistry, Geophysics, Geosystems*, 18(3), 1053–1064. <https://doi.org/10.1002/2016GC006715>
- Druitt, T. H., Edwards, L., Mellors, R. M., Pyle, D. M., Sparks, R. S. J., Lanphere, M., et al. (1999). *Santorini Volcano* (Vol. 19). Memoir-Geological Society of London.
- Druitt, T. H., Kutterolf, S., Ronge, T. A., & the Expedition 398 Scientists. (2024). *Proceedings of the International Ocean Discovery Program, Hellenic Arc volcanic field* (Vol. 398). International Ocean Discovery Program. <https://doi.org/10.14379/iodp.proc.398.2024>
- Druitt, T., Kutterolf, S., Ronge, T. A., Hübscher, C., Nomikou, P., Preine, J., et al. (2024). Giant offshore pumice deposit records a shallow submarine explosive eruption of ancestral Santorini. *Communications Earth and Environment*, 5(1), 24. <https://doi.org/10.1038/s43247-023-01171-z>
- Druitt, T. H., Kutterolf, S., Ronge, T. A., Beethe, S., Bernard, A., Berthod, C., et al. (2024). Site U1589. In T. H. Druitt, S. Kutterolf, & T. A. Ronge, & the Expedition 398 Scientists, Hellenic Arc Volcanic Field (Eds.) *Proceedings of the international ocean discovery program*. (Vol. 398). <https://doi.org/10.14379/iodp.proc.398.103.2024>
- Erickson, A. J., & Von Herzen, R. P. (1978). *Down-hole temperature measurements*. (Vol. 42A). Deep Sea Drilling Project. <https://doi.org/10.2973/dsdp.proc.42-1.143.1978>
- Fisher, A. T., Villinger, H., & Heesemann, M. (2007). *User manual for the third-generation, advanced piston corer temperature tool (APCT-3)*. Integrated Ocean Drill. Program.
- Forster, A., & Merriam, D. F. (1999). *Geothermics in basin analysis*. Springer Science. <https://doi.org/10.1007/978-1-4615-4751-8>
- Global Heat Flow Data Assessment Group, Fuchs, S., Neumann, F., Norden, B., Balkan-Pazvantoglu, E., Elbarbary, S., et al. (2024). The global heat flow database: Release 2024. *GFZ Data Services*. <https://doi.org/10.5880/figeo.2024.014>
- Hacker, B. R., Kelemen, P. B., & Behn, M. D. (2011). Differentiation of the continental crust by reamination. *Earth and Planetary Science Letters*, 307(3–4), 501–516. <https://doi.org/10.1016/j.epsl.2011.05.024>
- Hannington, M., Petersen, S., Nomikou, P., Wind, S., Heinath, V., Lange, S., et al. (2018). RV POSEIDON Fahrtbericht/Cruise report POS510–ANYDROS: Rifting and hydrothermal activity in the cyclades back-arc Basin, Catania (Italy)–Heraklion (Greece) 06.03.2017–29.03.2017. *GEOMAR Report, N. Series 043*. GEOMAR Helmholtz-Zentrum für Ozeanforschung, Kiel, Germany. https://doi.org/10.3289/geomar_rep_ns_43_2018
- Harris, R. N., Grevemeyer, I., Ranero, C. R., Villinger, H., Barckhausen, U., Henke, T., et al. (2010). Thermal regime of the costa rican convergent margin: 1. Along-Strike variations in heat flow from probe measurements and estimated from bottom-simulating reflectors. *Geochemistry, Geophysics, Geosystems*, 11(12). <https://doi.org/10.1029/2010GC003272>
- Hasterok, D., Gard, M., & Webb, J. (2018). On the radiogenic heat production of metamorphic, igneous, and sedimentary rocks. *Geoscience Frontiers*, 9(6), 1777–1794. <https://doi.org/10.1016/j.gsf.2017.10.012>
- Hayes, A., Kucera, M., Kallel, N., Sbaffi, L., & Rohling, E. J. (2005). Glacial Mediterranean Sea surface temperatures based on planktonic foraminiferal assemblages. *Quaternary Science Reviews*, 24(7–9), 999–1016. <https://doi.org/10.1016/j.quascirev.2004.02.018>
- Heath, B. A., Hooft, E. E. E., Toomey, D. R., Papazachos, C. B., Nomikou, P., Paulatto, M., et al. (2019). Tectonism and its relation to magmatism around Santorini Volcano from upper crustal P wave velocity. *Journal of Geophysical Research: Solid Earth*, 124(10), 10610–10629. <https://doi.org/10.1029/2019JB017699>
- Heesemann, M., Villinger, H., Fisher, A. T., Tréhu, A. M., & White, S. (2008). Data report: Testing and deployment of the new APCT-3 tool to determine in situ temperatures while piston coring. *Advances in the acquisition and processing of subseafloor temperature and pressure data and their interpretation in the context of convergent margin processes*, 21. <https://doi.org/10.2204/iodp.proc.311.108.2006>
- Hooft, E. E., Nomikou, P., Toomey, D. R., Lampridou, D., Getz, C., Christopoulou, M. E., et al. (2017). Backarc tectonism, volcanism, and mass wasting shape seafloor morphology in the Santorini-Christiana-Amorgos region of the Hellenic Volcanic Arc. *Tectonophysics*, 712, 396–414. <https://doi.org/10.1016/j.tecto.2017.06.005>
- Hornbach, M. J., Kühn, M., Freudenthal, T., Graw, J., Berndt, C., Huhn-Freher, K., et al. (2024). New heat flow measurements offshore Montserrat: Advective heat flow detected via MeBo borehole temperature logging. *Journal of Geophysical Research: Solid Earth*, 129(9), e2023JB028651. <https://doi.org/10.1029/2023JB028651>
- Hübscher, C., Ruhnau, M., & Nomikou, P. (2015). Volcano-tectonic evolution of the polygenetic Kolumbo submarine volcano/Santorini (Aegean Sea). *Journal of Volcanology and Geothermal Research*, 291, 101–111. <https://doi.org/10.1016/j.jvolgeores.2014.12.020>
- Hutchison, I. (1985). The effects of sedimentation and compaction on oceanic heat flow. *Geophysical Journal International*, 82(3), 439–459. <https://doi.org/10.1111/j.1365-246X.1985.tb05145.x>
- Jutzeler, M., Clark, A. S., Manga, M., McIntosh, I., Druitt, T., Kutterolf, S., & Ronge, T. A. (2025). Data report: Coring disturbances in advanced piston cores from IODP expedition 398, Hellenic Arc volcanic field. *Proceedings of the International Ocean Discovery Program*, 398. <https://doi.org/10.14379/iodp.proc.398.203.2025>
- Jutzeler, M., White, J. D. L., Talling, P. J., McCanta, M., Morgan, S., Le Friant, A., & Ishizuka, O. (2014). Methods for identifying coring disturbance in IODP piston cores and implications for volcanic events offshore Montserrat and deep sea record of Missoula mega-floods. *Geochemistry Geophysics Geosystem*, 15(9), 3572–3590. <https://doi.org/10.1002/2014GC005447>
- Karstens, J., Crutchley, G., Elger, J., Kühn, M., Schmid, F., Dalla Valle, G., & Nomikou, P. (2020). R/V Poseidon Cruise Report 538-THESEUS Tsunami hazard of explosive submarine eruptions. 7th October–28th October 2019, Cartagena (Spain)–Heraklion (Greece). https://doi.org/10.3289/cr_pos538

- Karstens, J., Crutchley, G. J., Hansteen, T. H., Preine, J., Carey, S., Elger, J., et al. (2023). Cascading events during the 1650 tsunamigenic eruption of Kolumbo volcano. *Nature Communications*, 14(1), 6606. <https://doi.org/10.1038/s41467-023-42261-y>
- Karstens, J., Preine, J., Carey, S., Bell, K. L., Nomikou, P., Hübscher, C., et al. (2023). Formation of undulating seafloor bedforms during the minoan eruption and their implications for eruption dynamics and slope stability at Santorini. *Earth and Planetary Science Letters*, 616, 118215. <https://doi.org/10.1016/j.epsl.2023.118215>
- Kuhnt, T., Schmiedl, G., Ehrmann, W., Hamann, Y., & Andersen, N. (2008). Stable isotopic composition of Holocene benthic foraminifera from the Eastern Mediterranean Sea: Past changes in productivity and deep water oxygenation. *Palaeogeography, Palaeoclimatology, Palaeoecology*, 268(1–2), 106–115. <https://doi.org/10.1016/j.palaeo.2008.07.010>
- Kutterolf, S., Druitt, T., Ronge, T., Beethe, S., Bernard, A., Berthod, C., et al. (2024). Expedition 398 methods. *Proceedings of the International Ocean Discovery Program*, 398. <https://doi.org/10.14379/iodp.proc.398.102.2024>
- Makris, J., Papoulia, J., & Yegorova, T. (2013). A 3-D density model of Greece constrained by gravity and seismic data. *Geophysical Journal International*, 194(1), 1–17. <https://doi.org/10.1093/gji/ggt059>
- Manga, M. (1998). Advective heat transport by low-temperature discharge in the Oregon Cascades. *Geology*, 26(9), 799–802. [https://doi.org/10.1130/0091-7613\(1998\)026<0799:AHTBLT>2.3.CO](https://doi.org/10.1130/0091-7613(1998)026<0799:AHTBLT>2.3.CO)
- Manga, M. (2025). Finite difference model for the subsurface temperature distribution in the Anhydros Basin [Software]. *Zenodo*. <https://doi.org/10.5281/zenodo.15283876>
- Manga, M., Hornbach, M. J., Le Friant, A., Ishizuka, O., Stronck, N., Adachi, T., et al. (2012). Heat flow in the lesser antilles island arc and adjacent back arc Grenada basin. *Geochemistry, Geophysics, Geosystems*, 13(8). <https://doi.org/10.1029/2012GC004260>
- McVey, B. G., Hooft, E. E. E., Heath, B. A., Toomey, D. R., Paulatto, M., Morgan, J. V., et al. (2020). Magma accumulation beneath Santorini volcano, Greece, from P-wave tomography. *Geology*, 48(3), 231–235. <https://doi.org/10.1130/G47127.1>
- Neumann, F., Negrete-Aranda, R., Harris, R. N., Contreras, J., Galerne, C. Y., Peña-Salinas, M. S., & Zhuang, G. (2023). Heat flow and thermal regime in the Guaymas Basin, Gulf of California: Estimates of conductive and advective heat transport. *Basin Research*, 35(4), 1308–1328. <https://doi.org/10.1016/j.palaeo.2008.07.010>
- Nomikou, P., Carey, S., Papanikolaou, D., Bell, K. C., Sakellariou, D., Alexandri, M., & Bejelou, K. (2012). Submarine volcanoes of the Kolumbo volcanic zone NE of Santorini caldera, Greece. *Global and Planetary Change*, 90, 135–151. <https://doi.org/10.1016/j.gloplacha.2012.01.001>
- Nomikou, P., Hübscher, C., & Carey, S. (2019). The Christiana–Santorini–Kolumbo volcanic field. *Elements: An International Magazine of Mineralogy, Geochemistry, and Petrology*, 15(3), 171–176. <https://doi.org/10.2138/gselements.15.3.171>
- Nomikou, P., Hübscher, C., Papanikolaou, D., Farangitakis, G. P., Ruhnau, M., & Lampridou, D. (2018). Expanding extension, subsidence and lateral segmentation within the Santorini–Amorgos basins during Quaternary: Implications for the 1956 Amorgos events, central-south Aegean Sea, Greece. *Tectonophysics*, 722, 138–153. <https://doi.org/10.1016/j.tecto.2017.10.016>
- Nomikou, P., Hübscher, C., Ruhnau, M., & Bejelou, K. (2016). Tectono-stratigraphic evolution through successive extensional events of the Anhydros Basin, hosting Kolumbo volcanic field at the Aegean Sea, Greece. *Tectonophysics*, 671, 202–217. <https://doi.org/10.1016/j.tecto.2016.01.021>
- Nomikou, P., Papanikolaou, D., Alexandri, M., Sakellariou, D., & Rousakis, G. (2013). Submarine volcanoes along the Aegean volcanic arc. *Tectonophysics*, 597, 123–146. <https://doi.org/10.1016/j.tecto.2012.10.001>
- Pasquale, V., Verdoya, M., & Chiozzi, P. (2001). Radioactive heat generation and its thermal effects in the Alps–Apennines boundary zone. *Tectonophysics*, 331(3), 269–283. [https://doi.org/10.1016/S0040-1951\(00\)00294-8](https://doi.org/10.1016/S0040-1951(00)00294-8)
- Pasquale, V., Verdoya, M., & Chiozzi, P. (2005). Thermal structure of the Ionian slab. *Pure and Applied Geophysics*, 162(5), 967–986. <https://doi.org/10.1007/s00024-004-2651-x>
- Pollack, H. N., Hurter, S. J., & Johnson, J. R. (1993). Heat flow from the earth's interior: Analysis of the global data set. *Reviews of Geophysics*, 31(3), 267–280. [https://doi.org/10.1016/S0040-1951\(00\)00294-8](https://doi.org/10.1016/S0040-1951(00)00294-8)
- Preine, J., Crutchley, G., Hübscher, C., Manga, M., Tominaga, M., Beethe, S., et al. (2025). Data report: Core-seismic integration and time-depth relationships at IODP expedition 398 Hellenic Arc volcanic field sites, and the expedition 398 scientists, Hellenic Arc volcanic field. In (Eds.), T. H. Druitt, S. Kutterolf, & T. A. Ronge *Proceedings of the International Ocean Discovery Program*. (Vol. 39). <https://doi.org/10.14379/iodp.proc.398.201.2025>
- Preine, J., Hübscher, C., Karstens, J., & Nomikou, P. (2022). Volcano-Tectonic evolution of the Christiana-Santorini-Kolumbo rift zone. *Tectonics*, 41(11), e2022TC007524. <https://doi.org/10.1029/2022TC007524>
- Preine, J., Karstens, J., Hübscher, C., Nomikou, P., Schmid, F., Crutchley, G. J., et al. (2022). Spatio-temporal evolution of the Christiana-Santorini-Kolumbo volcanic field, Aegean Sea. *Geology*, 50(1), 96–100. <https://doi.org/10.1130/G49167.1>
- Rudnick, R. L., & Fountain, D. M. (1995). Nature and composition of the continental crust: A lower crustal perspective. *Reviews of geophysics*, 33(3), 267–309. <https://doi.org/10.1029/95RG01302>
- Rybach, L. (1988). Determination of heat production rate. In (Eds.), R. Hanel, L. Rybach, & L. Stegna *Handbook of terrestrial heat flow density determination* (pp. 125–142). Kluwer.
- Taylor, S. R., & McLennan, S. M. (1995). The geochemical evolution of the continental crust. *Reviews of Geophysics*, 33(2), 241–265. <https://doi.org/10.1029/95RG00262>
- Tierney, J. E., Zhu, J., King, J., Malevich, S. B., Hakim, G. J., & Poulsen, C. J. (2020). Glacial cooling and climate sensitivity revisited. *Nature*, 584(7822), 569–573. <https://doi.org/10.1038/41586-020-2617-x>